Complete density calculations of q-state Potts and clock models: Reentrance of interface densities under symmetry breaking

Article *in* Physical Review E · December 2020

DOI: 10.1103/PhysRevE.102.062135

CITATIONS
18

READS
207

2 authors, including:

Erbil Can Artun
TÜBİTAK TBAE
17 PUBLICATIONS **35** CITATIONS

SEE PROFILE

Complete density calculations of q-state Potts and clock models: Reentrance of interface densities under symmetry breaking

E. Can Artun [1] and A. Nihat Berker[1,2]

[1]*Faculty of Engineering and Natural Sciences, Kadir Has University, Cibali, Istanbul 34083, Turkey*

[2]*Department of Physics, Massachusetts Institute of Technology, Cambridge, Massachusetts 02139, USA*

(Received 27 September 2020; accepted 17 November 2020; published 16 December 2020)

All local bond-state densities are calculated for q-state Potts and clock models in three spatial dimensions, $d = 3$. The calculations are done by an exact renormalization group on a hierarchical lattice, including the density recursion relations, and simultaneously are the Migdal-Kadanoff approximation for the cubic lattice. Reentrant behavior is found in the interface densities under symmetry breaking, in the sense that upon lowering the temperature, the value of the density first increases and then decreases to its zero value at zero temperature. For this behavior, a physical mechanism is proposed. A contrast between the phase transition of the two models is found and explained by alignment and entropy, as the number of states q goes to infinity. For the clock models, the renormalization-group flows of up to 20 energies are used.

DOI: 10.1103/PhysRevE.102.062135

I. INTRODUCTION: TOTAL RENORMALIZATION-GROUP SOLUTION OF TWO FAMILIES OF MODELS

Although originally introduced for critical phenomena, renormalization-group calculation gives the total thermodynamics of a system at and away from phase transitions [1]. To effect this, the recursion relations of the local densities are needed, causing the calculation to be more complicated than that for phase boundaries and critical exponents. This calculation is carried out here for two families of models, namely the Potts [2–4] and clock models [5], each with q states on a hierarchical lattice [1,6,7] in three spatial dimensions, $d = 3$. The calculation is exact for the hierarchical lattice and is considered approximate for a cubic lattice [8,9]. The temperature functions and symmetry-breaking behaviors of dozens of local densities are derived, and interesting behaviors are found and explained, such as a reentrance behavior in the interface densities. The models are similarly defined but they exhibit different behaviors, such as the q saturation of the magnetization and the phase transitions as q goes to infinity, which is also explained.

II. POTTS AND CLOCK MODELS, AND DENSITIES CALCULATION

A. The q-state models and their set of densities

These general q-state models are simply defined by the following Hamiltonians. For the Potts models,

$$-\beta\mathcal{H} = \sum_{\langle ij\rangle} J\delta(s_i s_j), \tag{1}$$

where $\beta = 1/k_B T$. At site i, the spin $s_i = a, b, \ldots$ can be in q different states, the delta function $\delta(s_i s_j) = 1(0)$ for $s_i = s_j (s_i \neq s_j)$, and $\langle ij\rangle$ denotes summation over all nearest-neighbor pairs of sites. For the clock models,

$$-\beta\mathcal{H} = \sum_{\langle ij\rangle} J\cos(\vec{s}_i \cdot \vec{s}_j), \tag{2}$$

where at site i the spin $\vec{s}_i$ can point in q different directions $\theta_i = 2\pi n_i/q$ in the xy plane, with $n_i = 0, 1, \ldots, q-1$ providing the q different possible states. The limit $q \to \infty$ of the clock model gives the XY model, which we also explore here, with results (physically explainably) quite different from the $q \to \infty$ limit of the Potts model (Fig. 1).

Our aim is to calculate all of the bond-state densities [there are $q(q+1)/2$ of them],

$$U(n_i n_j) = \langle \delta(s_i n_i)\delta(s_j n_j)\rangle, \tag{3}$$

where (i, j) are the sites on each end of the bond, and n_i designates one of q possible states of the spin s_i. These bond-state densities are obtained from the partition function Z,

$$U(n_i n_j) = \frac{1}{N}\frac{\partial \ln Z}{\partial E(n_i n_j)}, \tag{4}$$

where N is the number of nearest-neighbor pairs in the system, and $E(n_i n_j)$ is the energy assigned to the bond when its sites are in states (n_i, n_j). Before any renormalization, these bond energies are given by Eqs. (1) and (2),

$$E(n_i n_j) = J\delta(n_i n_j) \quad \text{and} \quad J\cos(2\pi(n_i - n_j)/q), \tag{5}$$

for the Potts and clock models, respectively. The $E(n_i n_j)$ are the (large number of; see below) renormalization-group flow variables, and Eqs. (5) give the initial conditions, parametrized by temperature J^{-1}, of the renormalization-group flows. The forms in Eqs. (5) are of course not conserved during the flows.

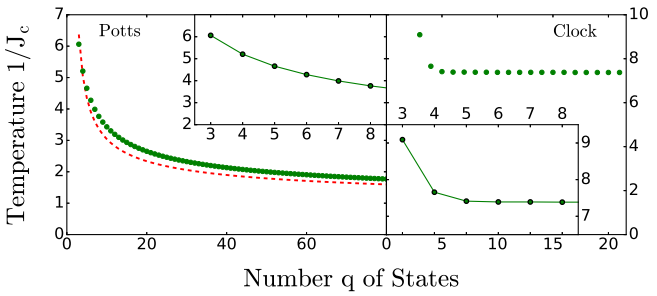

FIG. 1. Calculated critical temperatures J_c^{-1} of the Potts and clock models as a function of the number of states q in $d = 3$. From this figure and from Table I, it is seen that the clock model quickly (at as low as $q = 5$) settles to its $q = \infty$ (which is the XY model) value of $J_c^{-1} = 7.4$. The dashed line for the Potts critical temperatures is $J_c^{-1} = 7/\ln(q)$, derived here for strong coupling.

B. Energy recursion relations of the renormalization group

For our renormalization-group calculation, we use the Migdal-Kadanoff approximation, which, as shown in Fig. 2(a), consists in bond-moving followed by decimation [8,9]. This operation is equivalent to constructing the $q \times q$ transfer matrix $T(n_i n_j) = \exp(E(n_i n_j))$, taking the b^{d-1}th power of each element of the matrix (this is bond-moving) and multiplying the resulting matrix with itself (this is decimation). For numerical convenience at the low-temperature sink of the flows, after every decimation (and before first starting the first renormalization), we subtract $E(aa)$ (for the Potts model) or $E(00)$ (for the clock model) from all $E(n_i n_j)$, thus setting $E(aa) = 0$ or $E(00) = 0$ and introducing the additive constant NG in the Hamiltonian, which has the renormalization-group recursion relation

$$G' = b^d G + \tilde{G}, \tag{6}$$

where, here and everywhere, a prime refers to the renormalized system, the first term is the additive constants that the renormalized bond inherits from the b^d bonds it replaces, and

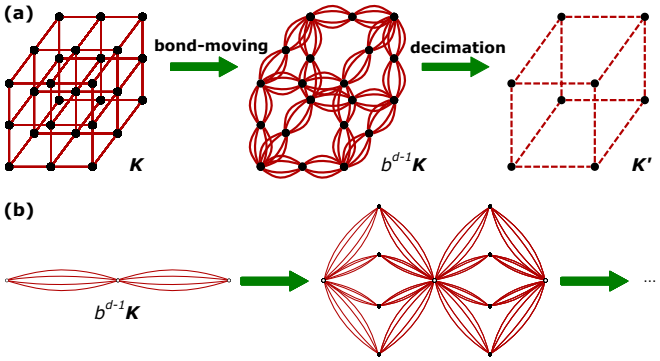

FIG. 2. (a) Migdal-Kadanoff approximate renormalization-group transformation for the $d = 3$ cubic lattice with the length-rescaling factor of $b = 2$. (b) Construction of the $d = 3, b = 2$ hierarchical lattice for which the Migdal-Kadanoff recursion relations are exact. The renormalization-group solution of a hierarchical lattice proceeds in the opposite direction of its construction.

the second term comes from compensating for the subtraction of $E(aa)$ or $E(00)$. These recursion relations are then in terms of the elements [or equivalently their logarithms $E(n_i n_j) = \ln(T(n_i n_j))$] of the diagonal and upper left triangle of the transfer matrix (since this matrix is symmetrical). The number of these elements can be somewhat reduced by noting those identically equal by symmetry and not to be distinguished by possible spontaneous symmetry breaking, as is illustrated for the clock models below, but it will be seen that the number of the flow variables for the clock models increases rapidly with q. A large q calculation, such as the one we perform here for $q = 360$ to probe the $q \to \infty$ XY model limit, is best carried out by directly performing numerically the matrix operations described above on the 360×360 transfer matrix. By contrast, for any q, by using the (partially broken under ordering) permutation symmetry of the Potts variables, we can reduce the number of renormalization-group flow variables to four, which makes it possible to treat any q, including $q = \infty$, as seen below. The recursion relations obtained by the Migdal-Kadanoff approximation are exactly applicable to the exact solution of the hierarchical lattice shown in Fig. 2(b) [1,6,7]. Thus, a "physically realizable" and therefore robust approximation is used. Physically realizable approximations have been used in polymers [10,11], disordered alloys [12], and turbulence [13]. Recent works using exactly soluble hierarchical lattices are in Refs. [14–19].

C. Density recursion relations of the renormalization group

In each renormalization-group transformation, the densities obey the recursion relation

$$\mathbf{U} = b^{-d}\mathbf{U}' \cdot \mathbf{R}, \tag{7}$$

where the densities $\mathbf{U} \equiv [1, U(n_i n_j)]$ are conjugate to the fields $\mathbf{E} \equiv [G, E(n_i n_j)]$, and the recursion matrix is $\mathbf{R} = \partial\mathbf{E}'/\partial\mathbf{E}$. The exact Eq. (7) is obtained by using the derivative chain rule on $\mathbf{U} = (1/N)\partial \ln Z/\partial\mathbf{E}$, where Z is the partition function and N is the number of nearest-neighbor pairs of spins, and it is used to calculate densities from renormalization-group theory [1,20,21]. In these defined vectors, the $E(aa)$ or $E(00)$ and $U(aa)$ or $U(00)$ are missing, since these energies are set to zero by the additive constant and therefore do not recur. $U(aa)$ and $U(00)$ are found from the sum rule $\Sigma_{n_i,n_j} U(n_i n_j) = 1$. The other densities are calculated by iterating Eq. (7) until a stable fixed point (the sink of the thermodynamic phase) is reached. The densities $\mathbf{U}^*$ at the sink are the left eigenvectors of $\mathbf{R}$ with eigenvalue b^d and conclude the calculation by insertion to the right-hand side of Eq. (7). These will be discussed below specifically for each model. The unstable fixed point dividing the renormalization-group flows to the phase sinks, parametrized by J, yields the phase transition temperatures given in Fig. 1 and Table I.

III. RESULTS: q-STATE POTTS MODELS

A. Potts recursion relations

Because of the permutation symmetry of the model, namely that given the δ function, with respect to a given state, all other states are equivalent (unlike the clock model involving the product of slightly or more aligned vectors), the

TABLE I. Calculated critical temperatures of the q-state Potts and clock models. The clock-model results have been found numerically by doing the sums in the renormalization-group decimation over a very large number of states, up to $q = 360$.

q	Potts J_c^{-1}	Clock J_c^{-1}
3	6.062	9.093
4	5.206	7.661
5	4.660	7.416
6	4.277	7.395
7	3.990	7.391
8	3.764	7.388
10	3.431	7.384
15	2.936	7.381
20	2.652	7.379
360	1.278	7.377
∞	$7/\ln(q)$	

$q \times q$ transfer matrix manipulations of the recursion relations given above can be reduced to four simple equations,

$$\begin{aligned} e^{E'(a\bar{b})+\tilde{G}} &= x(a\bar{b}) + x(a\bar{b})x(\bar{b}\bar{b}) + (q-2)x(a\bar{b})x(\bar{b}\bar{c}), \\ e^{E'(\bar{b}\bar{b})+\tilde{G}} &= x(a\bar{b})^2 + x(\bar{b}\bar{b})^2 + (q-2)x(\bar{b}\bar{c})^2, \\ e^{E'(\bar{b}\bar{c})+\tilde{G}} &= x(a\bar{b})^2 + 2x(\bar{b}\bar{b})x(\bar{b}\bar{c}) + (q-3)x(\bar{b}\bar{c})^2, \\ e^{\tilde{G}} &= 1 + (q-1)x(a\bar{b})^2, \end{aligned} \tag{8}$$

where the Potts state a has been singled out for possible spontaneous symmetry breaking, $\bar{b}$ represents any Potts state that is not a, and $\bar{c}$ represents any Potts state that is not a or the state in $\bar{b}$, and $x(a\bar{b}) \equiv e^{b^{d-1}E(a\bar{b})}$, etc. In the latter equation, the factor b^{d-1} represents bond-moving, and Eqs. (8) bring about the decimation with the bond-moved energies. The recursion matrix $\mathbf{R}$ is the 4×4 derivative matrix of Eqs. (8), and the density calculations can be done for any number of states q, including infinity. By a derivative matrix, we mean the derivatives of the renormalized quantities with respect to the unrenormalized quantities.

The recursion relations of Eqs. (8) flow to one of two phase sinks. On the high-temperature side, the sink of the disordered phase is

$$E(aa)^* = E(a\bar{b})^* = E(\bar{b}\bar{b})^* = E(\bar{b}\bar{c})^* = 0, \tag{9}$$

where * denotes the fixed point value. The left eigenvector, with eigenvalue b^d, of the recursion matrix $\mathbf{R}$ at this sink is

$$\begin{aligned} \mathbf{U}^* &= [1, U(a\bar{b})^*, U(\bar{b}\bar{b})^*, U(\bar{b}\bar{c})^*] \\ &= [1, \langle\delta(s_i a)\delta(s_j\bar{b})\rangle + \langle\delta(s_i\bar{b})\delta(s_j a)\rangle, \\ &\quad \langle\delta(s_i\bar{b})\delta(s_j\bar{b}\rangle, \langle\delta(s_i\bar{b})\delta(s_j\bar{c})\rangle] \\ &= [1, 2(q-1)/q^2, (q-1)/q^2, (q-1)(q-2)/q^2]. \end{aligned} \tag{10}$$

Capping with Eq. (10) from left the repeated applications of Eq. (7), the densities $U(a\bar{b}), U(\bar{b}\bar{b}), U(\bar{b}\bar{c})$ are obtained over the entire temperature range of the high-temperature disordered phase. Finally,

$$U(ab) = U(a\bar{b})/U^*(a\bar{b}), \tag{11}$$

etc. gives the density for a specific pair of states (a, b).

On the low-temperature side, the sink of the ordered phase is

$$E(aa)^* = E(\bar{b}\bar{b})^* = 0, \quad E(a\bar{b})^* = E(\bar{b}\bar{c})^* \to -\infty. \tag{12}$$

A left eigenvector, with eigenvalue b^d, of the recursion matrix $\mathbf{R}$ at this sink is

$$\mathbf{U}^* = [1, 0, 0, 0]. \tag{13}$$

Calculation, as described after Eq. (10) above, gives the densities over the entire temperature range of the low-temperature ordered phase, showing spontaneous symmetry-breaking in favor of state a. This result is described in detail in the next subsection.

Another left eigenvector, with eigenvalue b^d, of the recursion matrix $\mathbf{R}$ at this sink is [1,1,0,0]. This eigenvector gives symmetry breaking in favor of one of the states $\bar{b}$, namely one of the states that is not a. With the permutation mapping of the Potts model, this leads to results that are identical to the results involving symmetry breaking in favor of a. A linear combination of these two degenerate eigenvectors is of course also an eigenvector with the eigenvalue b^d, physically corresponding to the macroscopic coexistence of differently symmetry-broken phases.

It is noteworthy that throughout the renormalization-group flows,

$$E(aa) = E(\bar{b}\bar{b}), \quad E(a\bar{b}) = E(\bar{b}\bar{c}). \tag{14}$$

However, these interactions have to be distinguished in the recursion relations, enabling construction of the 4×4 recursion matrix $\mathbf{R}$, to calculate distinctly $U(aa), U(\bar{b}\bar{b})$, and to see the symmetry breaking. This calculation is also going to lead to the full determination of the magnetization, as seen below.

B. Potts densities and interface density reentrance

The calculated nearest-neighbor densities of the q-state Potts models in $d = 3$ are given, for $q = 3, 4, 5, 6, 7, 10, 15, 20$, in Fig. 3. (For easy comparison, the densities for the clock models are given in the adjoining Fig. 4.) The upper curve is $U(aa)$ and $U(bb)$, which coincide in the disordered high-temperature phase and split in the low-temperature phase where symmetry is spontaneously broken in favor of state a. The lower curve is $U(ab)$ and $U(bc)$, which also coincide in the disordered high-temperature phase and split in the symmetry-broken low-temperature phase. It is seen that the interface density $U(ab)$, between the symmetry-breaking and non-symmetry-breaking states, exhibits reentrance as temperature is lowered in the ordered phase, first increasing in value and then receding to zero at zero temperature. In Fig. 5, for comparison, the densities are plotted together for the different q values (and similarly for the clock models in the adjoining Fig. 6). The interface density reentrance is pronounced in the low q states, but continues for high q. As temperature is lowered through the phase transition, the reentrance relies on the following: (i) Due to the increase

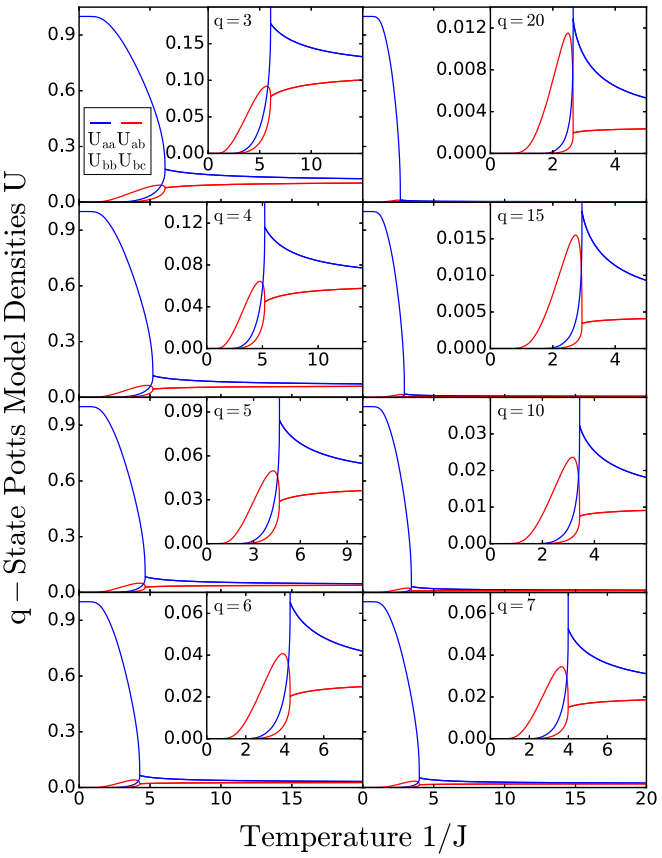

FIG. 3. The calculated nearest-neighbor densities of the q-state Potts models in $d = 3$. The upper curve on the right is U_{aa} and U_{bb}, which coincide in the disordered high-temperature phase and split in the low-temperature phase where symmetry is spontaneously broken in favor of state a. The lower curve on the right is U_{ab} and U_{bc}, which also coincide in the disordered high-temperature phase and split in the symmetry-broken low-temperature phase. The interface density U_{ab} exhibits reentrance as temperature is lowered in the ordered phase, first increasing in value and then receding to zero at zero temperature.

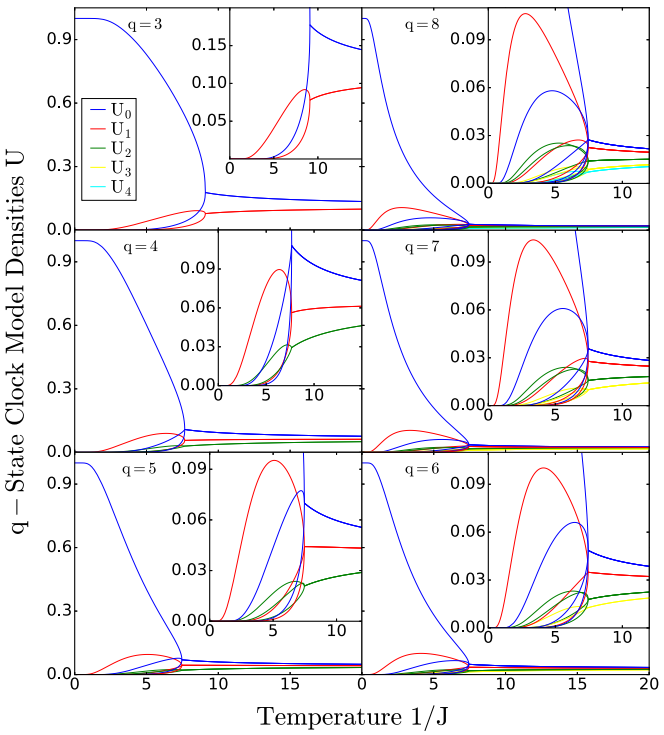

FIG. 4. The calculated nearest-neighbor densities of the q-state clock models in $d = 3$. The curves are for $U_m \equiv U_{k,k-m}$, for $k = 0, 1, \ldots, q-1$ and $m = 0, 1, \ldots,$ from the top down in each figure panel. Thus, m measures the angular difference $\theta_i - \theta_j = 2\pi m/q$ between the states of neighboring spins. For each m, the curves for different k coincide in the disordered high-temperature phase. In the low-temperature phase, for each m, the densities involving $k = 0$ and the densities involving $k > 0$ split under the symmetry breaking favoring the state 0. The interface densities involving $k = 0$ exhibit reentrance as temperature is lowered in the ordered phase, first increasing in value and then receding to zero at zero temperature.

in the sizes of the domains of the favored stated $s_i = a$, the numbers increase for the $(s_i = a, s_j \neq a)$ pairs at the boundaries of these domains. (ii) As the sizes of the domains of the favored state $s_i = a$ increase further, upon further lowering the temperature these domains merge, eliminating the boundaries. This reentrance is less pronounced for higher q, since the phase transition is at lower temperature and (ii) sets in before (i) develops.

Reentrance is the reversal of a thermodynamic trend as the system proceeds along one given thermodynamic direction. Since its observation in liquid crystals by Cladis [22], this at-first-glance strange phenomenon has attracted attention due to the need for a physical mechanistic explanation, which has been disparate in disparate systems. Thus, in liquid crystals the explanation has been the relief of close-packed dipolar frustration by positional fluctuations (librations) [23,24], in closed-loop binary liquid mixtures the explanation has been the asymmetric orientational degrees of freedom of the components [25], and in surface adsorption the explanation has been the buffer effect of the second layer [26]. In spin-glasses, where there is orthogonally bidirectional reentrance, the effect of frustration in both disordering and changing the nature of ordering (to spin-glass order) is the cause [27]. In cosmology, reentrance is due to high-curvature (black hole) gravity [28,29]. In the current case of Potts (and clock; see below) interfacial density, in lowering the temperature, when the system orders in favor of state a, the preponderance of the latter also increases its interface with the other states. However, as this preponderance increases further and in fact takes over the system, the other states are eliminated and their interface with a is thus also eliminated. This happens for all q-state Potts and clock models.

The calculated bond-state densities also readily yield magnetizations, which will be discussed in Sec. VI, as well as the different behaviors of the two models in the $q \to \infty$ limit.

IV. RESULTS: q-STATE CLOCK MODELS

Clock models do not have permutational symmetry, so the recursion relations for the diagonal and the top triangle of the $q \times q$ energies cannot be reduced to four equations [as in Eqs. (8) above]. Using the different symmetries for each q, the number of these energies that under renormalization

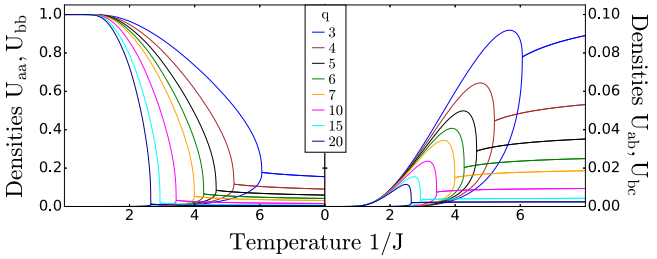

FIG. 5. Comparison with respect to the number of states $q = 3, 4, 5, 6, 7, 10, 15, 20$, from the top down in each panel, of the nearest-neighbor densities of the Potts models in $d = 3$. The right panel shows the curves for neighboring unlike states U_{ab} and U_{bc}, which coincide in the disordered high-temperature phase and split in the symmetry-broken low-temperature phase. The interface density U_{ab} exhibits reentrance as temperature is lowered in the ordered phase, first increasing in value and then receding to zero at zero temperature. This reentrance is pronounced in the low-q states and decreases for high q. The left panel shows the curves for the like-state neighbors U_{aa} and U_{bb}, which also coincide in the disordered high-temperature phase and split in the low-temperature phase where symmetry is spontaneously broken in favor of state a.

group recur separately can be reduced, but still increase with q, eventually numerically burdening the algebra.

A. Renormalization-group calculation and six-energy renormalization-group flows for $q = 4$

In the three-state clock model, since with respect to any one state the other two states are equivalent, for $q = 3$ the clock and Potts models are identical, up to a factor of $1 - \cos(2\pi/3) = 3/2$ in the coupling constant J.

In the four-state clock model, the six energies that need to recur separately under renormalization group are

$$\begin{aligned} &E(11) = E(33), \quad E(22), \quad E(12) = E(23), \\ &E(01) = E(03), \quad E(02), \quad E(13), \end{aligned} \tag{15}$$

where $E(mn)$ is the energy of neighboring spins with angles $2\pi m/q$ and $2\pi n/q$. The equalities result from the symmetries of the $q = 4$ state clock model, as the state with $m = 0$ is singled out for possible symmetry breaking. When, as we do here, the same energy label is assigned to different states that should have the same energy by symmetry, the derivative in Eq. (4) gives the sum of the densities of these states, as seen below.

The recursion relations are, similarly to Eqs. (8),

$$\begin{aligned} e^{E'(mn)+\widetilde{G}} &= \sum_{k=0}^{q-1} e^{b^{d-1}E(mk)+b^{d-1}E(kn)}, \\ e^{\widetilde{G}} &= \sum_{k=0}^{q-1} e^{b^{d-1}E(0k)+b^{d-1}E(k0)}. \end{aligned} \tag{16}$$

The renormalization-group flows and the calculation of the thermodynamic densities proceed as for the Potts models above. The recursion matrix is the 7×7 derivative matrix of $[G, E(mn)]$, where $E(mn)$ are the six energies of Eq. (15) and G is the additive constant as in Eq. (6), a captive variable of

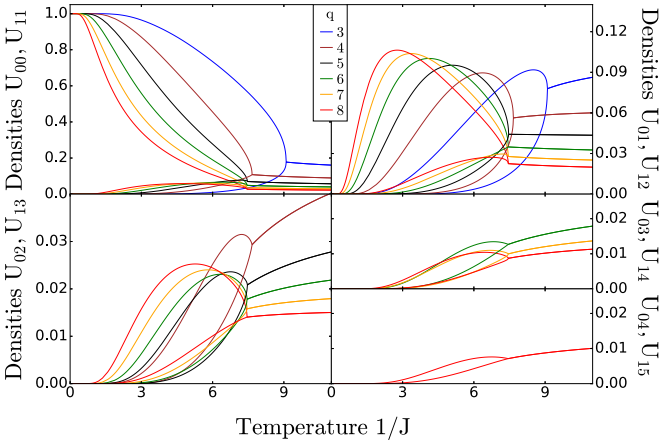

FIG. 6. Comparison with respect to the number of states $q = 3, 4, 5, 6, 7, 8$ of the nearest-neighbor densities of the clock models, $U_m \equiv U_{k,k-m}$ for $k = 0, 1$ and $m = 0, 1, \ldots,$ shown in decreasing q on the high-temperature side in each panel. m measures the angular difference $\theta_i - \theta_j = 2\pi m/q$ between neighboring spins. The top right panel shows the curves for neighboring unlike states with $m = 1$. The bottom left panel shows the curves with $m = 2$, and therefore $q = 4, 5, 6, 7, 8$. The bottom right upper panel shows the curves with $m = 3$, and therefore with $q = 6, 7, 8$. The bottom right lower panel shows the curves with $m = 4$, and therefore $q = 8$. For each m, the curves for different k coincide in the disordered high-temperature phase. In the low-temperature phase, for each m, the densities involving $k = 0$ and the densities involving $k > 0$ split under the symmetry breaking favoring the state 0. All interface densities involving $k = 0$ exhibit reentrance as temperature is lowered in the ordered phase, first increasing in value and then receding to zero at zero temperature.

the renormalization-group flows of the $E(mn)$. By a derivative matrix, we again mean the derivatives of the renormalized quantities with respect to the unrenormalized quantities.

The left eigenvector with eigenvalue b^d of the recursion matrix at the phase sinks has the form $[1, \overline{U}(mn)]$, where $\overline{U}(mn)$ are the density sums conjugate to the recurring $E(mn)$. At the high-temperature disordered phase sink, all energies equal $E(00)$, namely zero, and $\overline{U}(mn) = z(mn)/q^2$, where $z(mN)$ is the degeneracy of $E(mn)$, namely $z = 2, 1, 4, 4, 2, 2$ for the energies in Eq. (15), also taking into account the degeneracy for label interchange when $m \neq n$. Repeated application of Eq. (7) then yields the six density sums $\overline{U}(mn)$ in the entire temperature range of the disordered phase. The densities for individual states are obtained from the sums by $\langle\delta(mn)\rangle = U(mn) = \overline{U}(mn)/z(mn)$. For example,

$$\begin{aligned} \overline{U}(01)/z(01) &= \langle[\delta(01) + \delta(10) + \delta(03) + \delta(30)]\rangle/4 \\ &= \langle\delta(01)\rangle = U(01). \end{aligned} \tag{17}$$

Thus, when we reduce the number of the recurring energies using symmetries as in Eq. (15) and label interchange symmetry, the renormalization-group calculation yields the density sum $\overline{U}(01)$, which is then subjected to Eq. (17). At the low-temperature sink, in the left eigenvector with eigenvalue b^d, all $\overline{U}(mn) = 0$, and therefore $U(00) = 1 - \Sigma_{mn}U(mn) = 1$, symmetry is broken in favor of state 0. Repeated application of Eq. (7) then yields the six density sums $\overline{U}(mn)$ in the

entire temperature range of the ordered phase. [The other left eigenvector with eigenvalue b^d is $\overline{U}(\overline{00}) = 1$, where $\overline{0}$ is a state other than 0, and all other recurring $\overline{U}(mn) = 0$, giving an equivalent phase and completing the picture of phase coexistence, as for the Potts models above.]

The calculated nearest-neighbor densities of the four-state clock model in $d = 3$ are shown in Fig. 4. The densities $U(00), U(11), U(33)$ coincide in the disordered high-temperature phase, and in the low-temperature phase $U(00)$ splits from $U(11), U(33)$ under the symmetry breaking favoring the state 0. Similarly, $U(01), U(03), U(12), U(23)$ coincide in the disordered high-temperature phase, and in the low-temperature phase $U(01), U(03)$ splits from $U(12), U(23)$ under the symmetry breaking. Similarly, $U(02), U(13)$ coincide in the disordered high-temperature phase, and in the low-temperature phase $U(02)$ splits from $U(13)$ under the symmetry breaking. The densities involving the 0 state split from their symmetric counterparts in the low-temperature phase, increasing their values. This is spontaneous symmetry breaking. Furthermore, the interface densities involving the 0 state exhibit reentrance as temperature is lowered in the ordered phase, first increasing in value and then receding to zero at zero temperature.

B. Renormalization-group flows of 8, 12, 15, and 20 energies for $q = 5, 6, 7, 8$

The calculations for $q = 5, 6, 7, 8$ are more extensive. Using symmetries grouping the same values of $|n - m|$, but grouping separately for positioning with respect to state 0, for the possibility of spontaneous symmetry breaking, $q = 5, 6, 7, 8$ have renormalization-group flows in 8, 12, 15, and 20 energies, respectively. These constitute very extensive renormalization-group calculations.

The results are shown in Fig. 4. Direct comparison between different q is shown in Fig. 6, showing a striking evolution with respect to q. The characteristic behavior is seen here as well. The curves are for $U_{k,k-m}$ for $k = 0, 1, \ldots, q-1$ and $m = 0, 1, \ldots$. Thus, m measures the angular difference $\theta_i - \theta_j = 2\pi m/q$ between the states of neighboring spins. For each m, the curves for different k coincide in the disordered high-temperature phase. In the low-temperature phase, for each m, the densities involving $k = 0$ and the densities involving $k > 0$ split under the spontaneous symmetry breaking favoring the state 0. The interface densities involving $k = 0$ exhibit reentrance as temperature is lowered in the ordered phase, first increasing in value and then receding to zero at zero temperature.

V. MAGNETIZATIONS AND INFINITE q (NON)SATURATION OF THE CRITICAL TEMPERATURE

The magnetizations M are directly obtained from the nearest-neighbor densities. For the Potts models,

$$M = \langle \delta(s_i a) \rangle = \sum_{m=0,n=0}^{q-1,q-1} U(mn)\, \delta(ma). \tag{18}$$

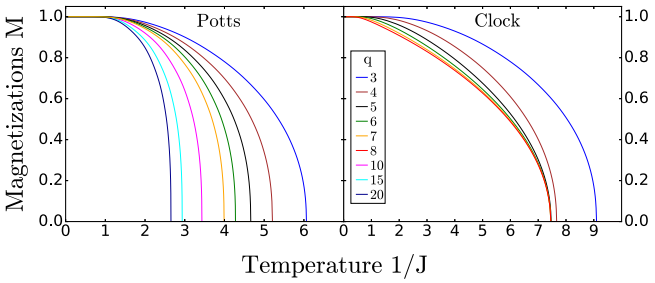

FIG. 7. Calculated magnetizations of the Potts and clock models as a function of temperature J^{-1} in $d = 3$ for different values of the number of states q. It is noteworthy that, in the clock models, the magnetization quickly (at as low as $q = 5$) settles to its $q = \infty$ (which is the XY model) value along the entire temperature range of the low-temperature ordered phase, not only at the value of J_c^{-1} as was seen above in Fig. 1 and Table I.

For the clock models,

$$M = \langle \cos(\theta_i) \rangle = \sum_{m=0,n=0}^{q-1,q-1} U(mn)\, \cos(2\pi m/q). \tag{19}$$

These equations are obtained by including a magnetic field term (to be taken to zero after differentiating) in the $E(mn)$, differentiating $\ln(Z)$ with respect to the magnetic field, and using the chain rule with $E(mn)$ as intermediary.

The results for the magnetizations and the critical temperatures are given in Figs. 1 and 7 and Table I. It should be noted that these results are exact for the $d = 3$ hierarchical lattice. They are approximate for the cubic lattice. Specifically, by allowing effective vacancies to be generated by the renormalization-group transformation, the Potts model transition correctly becomes first order for $q > 2$ [2–4].

It is of interest to see the magnetization curves for the clock models in Fig. 7 settle to their $q \to \infty$ value for as low as $q = 5$. This is of course reflected in the essentially constant value of the clock critical temperatures as q is increased.

Such is not the case for the Potts models. Directly writing down the recursion relation for J in Eq. (1),

$$J' = \ln\left[e^{2b^{d-1}J} + (q-1)\right] - \ln\left[2e^{b^{d-1}J} + (q-2)\right], \tag{20}$$

setting the fixed point condition $J' = J = J_c$, and expanding for large J and q, we find the critical temperatures

$$J_c^{-1} = 7/\ln(q). \tag{21}$$

This curve is plotted as a dashed curve in Fig. 1 and gives a good fit even for finite q. As $q \to \infty$, the critical temperature goes to zero.

There is a physical explanation for the contrast between the Potts and clock models. In the Potts models, the states neighboring $s_i = a$ do not contribute to the magnetization and they are entropically favored as q is increased. (In fact, in the permutationally symmetric Potts models, the concept of "neighboring" state has no meaning: every state is equally positioned with respect to a chosen state.) By contrast, in the clock models, the states neighboring $\theta_i = 0$ give almost a full contribution, namely $\langle \cos(2\pi n_i/q) \rangle$ to the magnetization, where $n_i \ll q$ for large q. Thus, in all spatial dimensions d, the

critical temperature for Potts models should go to zero inverse logarithmically as $q \to \infty$.

VI. CONCLUSION

In this study, we have calculated all of the bond-state densities of the q-state Potts and clock models in $d = 3$. This was done for all q for the Potts models by reducing the recursion relations to four, using symmetries, modulo singling out one state for possible spontaneous symmetry breaking, which happens for both models. Although the number of recursion relations in clock models can be reduced by symmetry, their number grows, for example to 20 different energies for our treated eight-state clock model. However, we have presented a robust method that would make the calculation for any number of states q feasible.

A reentrant behavior of all of the symmetry-broken interface densities was found for both models, and was physically explained. A surprising saturation with increasing q was found in the clock models, but not in the Potts models. We also found qualitatively different phase transition behaviors in the $q \to \infty$ limit, which was physically explained by entropy and alignment arguments.

ACKNOWLEDGMENTS

Support by the Kadir Has University Doctoral Studies Scholarship Fund and by the Academy of Sciences of Turkey (TÜBA) is gratefully acknowledged.

[1] A. N. Berker and S. Ostlund, J. Phys. C **12**, 4961 (1979).
[2] A. N. Berker, S. Ostlund, and F. A. Putnam, Phys. Rev. B **17**, 3650 (1978).
[3] B. Nienhuis, A. N. Berker, E. K. Riedel, and M. Schick, Phys. Rev. Lett. **43**, 737 (1979).
[4] D. Andelman and A. N. Berker, J. Phys. A **14**, L91 (1981).
[5] A. N. Berker and D. R. Nelson, Phys. Rev. B **19**, 2488 (1979).
[6] R. B. Griffiths and M. Kaufman, Phys. Rev. B **26**, 5022(R) (1982).
[7] M. Kaufman and R. B. Griffiths, Phys. Rev. B **30**, 244 (1984).
[8] A. A. Migdal, Zh. Eksp. Teor. Fiz. **69**, 1457 (1975) [Sov. Phys. JETP **42**, 743 (1976)].
[9] L. P. Kadanoff, Ann. Phys. (NY) **100**, 359 (1976).
[10] P. J. Flory, *Principles of Polymer Chemistry* (Cornell University Press, Ithaca, NY, 1986).
[11] M. Kaufman, Entropy **20**, 501 (2018).
[12] P. Lloyd and J. Oglesby, J. Phys. C **9**, 4383 (1976).
[13] R. H. Kraichnan, J. Math. Phys. **2**, 124 (1961).
[14] C. Monthus, J. Stat. Mech.: Theor. Exp. (2020) 013301.
[15] O. S. Sarıyer, Philos. Mag. **99**, 1787 (2019).
[16] P. A. Ruiz, Commun. Math. Phys. **364**, 1305 (2018).
[17] M. J. G. Rocha-Neto, G. Camelo-Neto, E. Nogueira, Jr., and S. Coutinho, Physica A **494**, 559 (2018).
[18] F. Ma, J. Su, Y. X. Hao, B. Yao, and G. G. Yan, Physica A **492**, 1194 (2018).
[19] S. Boettcher and S. Li, Phys. Rev. A **97**, 012309 (2018).
[20] E. Ilker and A. N. Berker, Phys. Rev. E **89**, 042139 (2014).
[21] B. Atalay and A. N. Berker, Phys. Rev. E **98**, 042125 (2018).
[22] P. E. Cladis, Phys. Rev. Lett. **35**, 48 (1975).
[23] R. R. Netz and A. N. Berker, Phys. Rev. Lett. **68**, 333 (1992).
[24] J. O. Indekeu, A. N. Berker, C. Chiang, and C. W. Garland, Phys. Rev. A **35**, 1371 (1987).
[25] C. A. Vause and J. S. Walker, Phys. Lett. A **90**, 419 (1982).
[26] R. G. Caflisch, A. N. Berker, and M. Kardar, Phys. Rev. B **31**, 4527 (1985).
[27] E. Ilker and A. N. Berker, Phys. Rev. E **87**, 032124 (2013).
[28] A. M. Frassino, D. Kubiznak, R. B. Mann, and F. Simovic, J. High Energy Phys. 09 (2014) 080.
[29] A. Dehghani, S. H. Hendi, and R. B. Mann, Phys. Rev. D **101**, 084026 (2020).